

Hang Ni¹ Weijia Zhang¹ Fei Wang^{2,3} Zehui Shao² Hao Liu¹

Abstract

Advances in multi-modal large language models (MLLMs) have inspired time series understanding and reasoning tasks, that enable natural language querying over time series, producing textual analyses of complex temporal dynamics. Recent attempts hybridize numerical time series with their visualized plots, facilitating precise value reasoning and visual structure comprehension for comprehensive time series understanding of MLLMs. However, effective cross-modal integration remains challenging due to fine-grained temporal misalignment across modalities and severe entanglement between shared and modality-specific semantics, which hinder localized interpretation and complementary reasoning. To address these issues, we propose **MADI**, a **multi-modal LLM** enhanced with fine-grained **alignment** and **disentangled interaction**, featuring (1) Patch-level Alignment, which enforces physically grounded fine-grained correspondence across heterogeneous modalities, (2) Discrete Disentangled Interaction, which separates modality-common semantics into compact discrete latents and adaptively synergizes the purified modality-unique information, and (3) Critical-token Highlighting, which emphasizes informative, query-relevant signals for robust reasoning. Experiments on synthetic and real-world benchmarks show that MADI consistently outperforms general-purpose LLMs and time-series-specialized MLLMs.

1. Introduction

Time series understanding and reasoning (TSUR) tasks aim to interpret natural language queries alongside uni- or multi-variate time series inputs, producing textual explanations or

¹The Hong Kong University of Science and Technology (Guangzhou) ²Institute of Computing Technology, Chinese Academy of Sciences ³University of Chinese Academy of Sciences. Correspondence to: Hao Liu <liuh@ust.hk>.

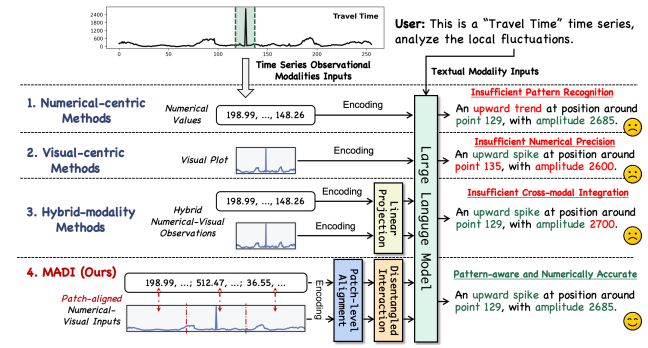


Figure 1. Comparison of multi-modal architectures.

analyses of temporal dynamics (Xie et al., 2025). Unlike classical time series tasks (e.g., forecasting, classification, anomaly detection) (Wang et al., 2024) which operate on uni-modal numerical inputs and yield task-specific outputs with limited flexibility and interpretability, TSUR supports interpretable, language-driven interactions between time series data and users via open-ended natural language dialogue. Such capabilities are crucial for human decision-making in real-world scenarios, including healthcare (Lan et al., 2025), finance (Chen et al., 2025), and industrial maintenance (Wang et al., 2025b).

With the rapid advancement of large language models (LLMs), TSUR tasks have become dominated by LLM-based paradigms, enabling flexible user queries and textual outputs. Beyond linguistic inputs, existing works primarily focus on *how to formulate time series into effective observational modalities* that can be jointly processed with language by LLMs. *Numerical-centric methods* directly feed raw time series values into LLMs as an additional modality (Wang et al., 2025a;b; Xie et al., 2025). While preserving precision, studies indicate that LLMs struggle to recognize high-level temporal structures like trends and periodicity (Liu et al., 2025c), reflecting a fundamental numerical-language modality gap induced by text-only LLM pre-training (Tan et al., 2024). In contrast, *visual-centric methods* convert time series into visual plots and leverage the strong visual processing abilities of multi-modal LLMs (MLLMs) (Liu et al., 2025c; Merrill et al., 2024; Zhang et al., 2025a). Although effective at capturing high-level temporal structures, these approaches often sacrifice fine-grained numerical details that are critical for precise temporal analysis (Xu et al.,

2025; Zhao et al., 2025). Recent hybrid approaches like GEM (Lan et al., 2025) attempt to combine numerical and visual modalities within MLLMs via token concatenation for comprehensive time series understanding. Despite these advances, effectively integrating these two observational modalities for MLLMs reveals two critical challenges:

(1) Fine-grained Cross-modal Alignment. Numerical values and their visual renderings reflect the same underlying physical signal, yet they are often encoded independently, leading to misaligned representations that hinder cross-modal reasoning. Moreover, vision-language pre-training gaps of MLLMs amplify this misalignment, preventing models from achieving the interpretive accuracy with numerical data that they attain in vision. Existing methods either rely on implicit alignment via linear projections (Lan et al., 2025), which can not enforce explicit physical correspondence, or perform series-level contrastive alignment (Dong et al., 2025), which overlooks fine-grained temporal variations (e.g., fluctuations, noise) and can induce localized hallucinations. Hence, a key challenge is to establish physically grounded, fine-grained alignment between numerical and visual modalities, providing a consistent semantic reference for accurate cross-modal understanding.

(2) Disentangled Cross-modal Interaction. Although alignment ensures fundamental cross-modal consistency, it is not sufficient for effective time series understanding without fully leveraging complementary strengths of visual patterns and numerical details. To integrate these unique features across modalities, existing approaches employ various multi-modal fusion and interaction strategies, such as feature concatenation (Lan et al., 2025), additive fusion (Zhong et al., 2025) and cross-attention (Liu et al., 2025b). However, numerical and visual modalities describe the same underlying signals, resulting in substantial information overlap entangled with the modality-unique semantics. Directly operating on full-modal representations often allows redundant, modality-shared content to dominate, diluting the unique contributions of each modality and limiting cross-modal synergy. This motivates the second challenge: how to disentangle shared and modality-specific semantics after alignment, and integrate complementary signals to achieve synergistic reasoning, rather than mere feature aggregation.

To address these challenges, we propose **MADI**, a multi-modal LLM (MLLM) for TSUR tasks, enhanced with fine-grained alignment and disentangled interaction across heterogeneous modalities. The distinctions between MADI and prior methods are highlighted in Figure 1. We first introduce a *Patch-level Alignment (PA)* module that performs fine-grained contrastive alignment between numerical time series and their visualized line plots at a patch granularity, ensuring physically grounded local correspondence for accurate cross-modal reasoning. To enhance MLLM

comprehension of numerical inputs, we further incorporate patch-wise textual captions derived from the time series, aligning numerical values with their textual descriptions. Together, these alignments ground numerical representations in the MLLM-compatible vision–language semantic space, facilitating robust multi-modal reasoning. Building on the aligned representations, we devise a *Discrete Disentangled Interaction (DDI)* module to exploit the complementary benefits of numerical precision and visual abstraction. To separate modality-unique semantics from modality-common redundancies, DDI introduces a compact discrete latent space via hierarchical vector quantization, capturing multi-scale, compact modality-common features to enhance disentanglement purity. The unique components are then integrated through cross-attention, enabling synergistic interaction while preventing interference from redundant shared signals. Finally, to enhance generalization, we introduce a lightweight *Critical-token Highlighting (CTH)* module that identifies informative, question-relevant tokens across modalities, and prepends them to the token sequences. By incorporating these modules into a pre-trained MLLM, MADI enables interpretable and flexible TSUR across diverse domains and query types, and extensive experiments demonstrate consistent improvement over both general-purpose LLMs and time-series-specialized baselines.

In summary, our contributions are threefold: (1) We propose a Patch-level Alignment (PA) module to enforce fine-grained physical consistency between numerical values and visual plots, preventing localized MLLM hallucinations. (2) We introduce a Discrete Disentangled Interaction (DDI) module to filter shared redundancies and leverage the complementarities of multi-modal signals for robust reasoning. (3) We conduct extensive experiments on synthetic and real-world data demonstrating the advances of MADI in TSUR.

2. Related Work

2.1. Multi-modal Methods for Classical Time Series Analysis

Recent studies explore augmenting time series with auxiliary modalities, such as text or images, to enhance classical analysis, particularly forecasting tasks. One line of research integrates numerical series with textual descriptions (Liu et al., 2025b) or exogenous contexts (Zhang et al., 2025b), typically via dual-branch architectures that encode each modality separately before fusing them for downstream tasks (Liu et al., 2024; Zhou et al., 2025; Liu et al., 2025b; Ding et al., 2025; Jiang et al., 2025). With the rise of LLMs, recent efforts enable LLMs to jointly process textual and numerical inputs, by either tokenizing numerical values (Gruver et al., 2023; Wang et al., 2025a), or aligning time series representations with LLM-compatible textual embeddings through contrastive learning (Zhang et al., 2025b), cross-

attention mechanisms (Jin et al., 2024; Liu et al., 2025d), or graph neural networks (Hu et al., 2025).

Another line further incorporates visual modalities derived from time series plots or auxiliary sources. For instance, Time-VLM (Zhong et al., 2025) visualizes series as heatmaps and generates textual summaries, which are fused with numerical inputs for forecasting. PIPE (Li et al., 2025) incorporates satellite imagery as physical cues to enhance typhoon intensity prediction. These approaches remain mostly task-specific and constrained by fixed output formats, limiting their applicability to flexible reasoning scenarios such as time series understanding and reasoning.

2.2. Time Series Understanding and Reasoning

Beyond classical analysis, time series understanding and reasoning (TSUR) emphasizes interpretable analyses of temporal dynamics under flexible natural language queries, leveraging LLMs. Existing approaches can be broadly classified as numerical-centric, visual-centric, and hybrid paradigms. Numerical-centric methods represent time series values as sequences of textual or continuous tokens (Wang et al., 2025a;b; Xie et al., 2025), preserving precision but often struggling with high-level temporal structures due to the text-centric pre-training of LLMs (Tan et al., 2024; Liu et al., 2025c). Visual-centric approaches (Liu et al., 2025c; Merrill et al., 2024; Zhang et al., 2025a) reframe time series analysis as a visual question-answering task, transforming the series into plots and leveraging advanced MLLMs (Liu et al., 2025c; Merrill et al., 2024; Zhang et al., 2025a). These methods can effectively capture high-level patterns, e.g., trend and periodicity, but sacrifice fine-grained numerical details (Xu et al., 2025; Zhao et al., 2025). Hybrid approaches, e.g., GEM (Lan et al., 2025), combine both modalities, but typically rely on simple concatenation and remain domain-specific (e.g., ECG), limiting the principled cross-modal alignment and interaction. Our work addresses these limitations with a generalizable MLLM that integrates numerical precision and visual abstractions via fine-grained alignment and disentangled cross-modal interaction, supporting diverse domains and flexible query types.

3. Preliminary

3.1. Problem Statement

Time series understanding and reasoning (TSUR) aim to analyze time series based on a natural language query and generate a textual answer. Formally, given a set of time series $\mathcal{X} = \{\mathbf{x}_1, \mathbf{x}_2, \dots, \mathbf{x}_{|\mathcal{X}|}\}$, where each $\mathbf{x}_i = (x_{i;1}, x_{i;2}, \dots, x_{i;T_i}) \in \mathbb{R}^{T_i}$ consists of T_i observations, along with textual inputs including a context C and a question Q , the objective is to learn a mapping $f : (\mathcal{X}, C, Q) \rightarrow A$, producing an answer A that explains or reasons about

the relevant information in \mathcal{X} with respect to Q .

3.2. Vector Quantization

Vector Quantization (VQ) (van den Oord et al., 2017) maps continuous features to a finite set of discrete prototypes, enabling compact, structured representations. Given input features $\mathbf{E} = [\mathbf{e}_1, \dots, \mathbf{e}_N]^\top \in \mathbb{R}^{N \times D}$ and a codebook $\mathcal{C} = \{\mathbf{c}_k\}_{k=1}^K \subseteq \mathbb{R}^D$, each feature is quantized via nearest-neighbor assignment: $\mathbf{q}_j = \arg \min_{\mathbf{c}_k \in \mathcal{C}} \|\mathbf{e}_j - \mathbf{c}_k\|_2^2$. To enable gradient-based optimization, VQ employs a straight-through estimator (STE) together with a commitment loss, resulting in the objective $\mathcal{L}_{\text{vq}} = \|\mathbf{e}_j - \text{sg}[\mathbf{q}_j]\|_2^2$, where $\text{sg}[\cdot]$ denotes the stop-gradient operator. The codebook is commonly updated using exponential moving average (EMA).

Residual Vector Quantization (RVQ) (Lee et al., 2022) extends VQ by sequentially quantizing residuals, increasing representation capacity. Using M codebooks $\{\mathcal{C}^{(m)}\}_{m=1}^M$, RVQ initializes $\mathbf{r}_j^{(0)} = \mathbf{e}_j$ and iteratively performs $\mathbf{q}_j^{(m)} = \arg \min_{\mathbf{c} \in \mathcal{C}^{(m)}} \|\mathbf{r}_j^{(m-1)} - \mathbf{c}\|_2^2$ and $\mathbf{r}_j^{(m)} = \mathbf{r}_j^{(m-1)} - \mathbf{q}_j^{(m)}$. The final quantized representation is $\mathbf{q}_j = \sum_{m=1}^M \mathbf{q}_j^{(m)}$.

4. Methodology

Figure 2 illustrates the overall architecture of MADI. It is built upon a pre-trained MLLM, reusing its vision encoder and LLM to perform time series understanding and reasoning (TSUR). Specifically, *Patch-level Alignment (PA)* first expands each time series as patch-aligned numerical, visual and textual modalities, aligning them in a consistent embedding space. Based on these aligned tokens, *Discrete Disentangled Interaction (DDI)* separates modality-shared and unique semantics for numerical and visual inputs and synergizes their complementarities. *Critical-token Highlighting (CTH)* then identifies informative, question-relevant tokens from the PA-aligned embeddings and prepends them to the DDI-fused multi-modal sequence. The resulting multi-modal tokens are concatenated with the textual input tokens and decoded by the LLM to generate the output.

4.1. Patch-level Alignment

To establish precise correspondence between numerical and visual modalities and enable accurate MLLM interpretation of numerical inputs, we propose a *Patch-level Alignment (PA)* module that enforces fine-grained, physically-grounded alignment among numerical, visual, and textual modalities. PA operates at a patch level and consists of three steps: (1) *patch-level modality expansion*, which constructs patch-aligned textual and visual counterparts; (2) *multi-modal encoding*, which embeds each modality independently; and (3) *contrastive alignment*, which employs patch-wise contrastive learning to reduce cross-modal representation gaps.

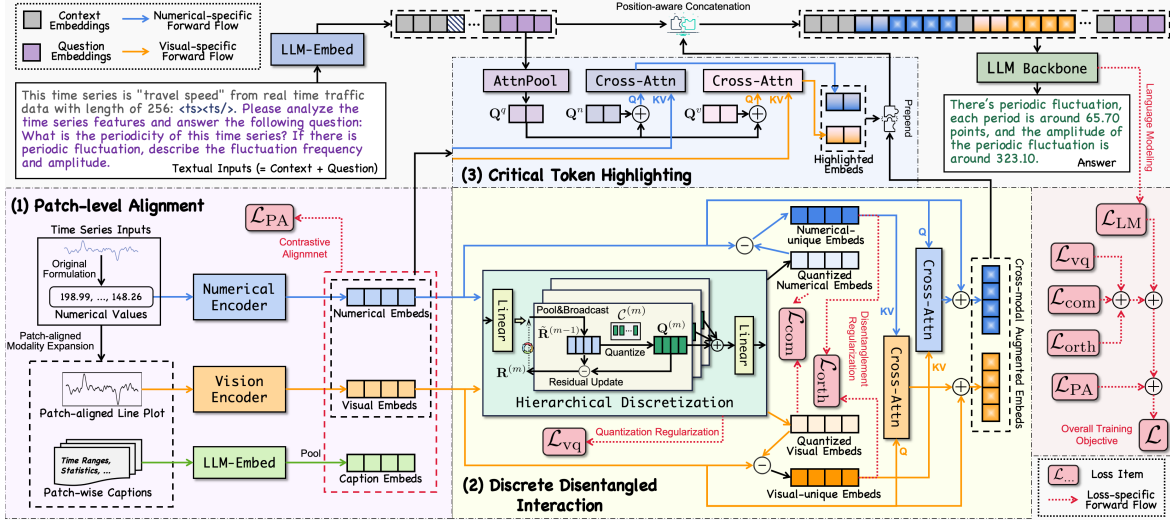


Figure 2. The model architecture of MADI.

4.1.1. PATCH-LEVEL MODALITY EXPANSION

Following (Nie et al., 2023), each time series \mathbf{x}_i can be divided into non-overlapping patches to enable efficient and robust temporal modeling: $\mathbf{P}_i^n = \text{Patching}(\mathbf{x}_i) \in \mathbb{R}^{\tilde{T}_i \times p^n}$, where $\tilde{T}_i = [T_i/p^n]$ denotes the number of patches, and p^n is the patch size of time series. Based on such a patch-level granularity, the numerical modality is then expanded with textual and visual modalities.

Patch-aligned Visualization. We render \mathbf{x}_i as a line plot with adaptive resolution $\tilde{T}_i \cdot p^v \times p^v$ (width \times height) where p^v is the patch size of the vision encoder in the backbone MLLM. We intentionally omit all decorative plotting elements (e.g., titles, axes, ticks, labels, and legends), thereby the resulting image \mathbf{I}_i can be patchified into $\mathbf{P}_i^v \in \mathbb{R}^{\tilde{T}_i \times p^v \times p^v}$, ensuring a one-to-one correspondence with numerical patches \mathbf{P}_i^n , and enabling fine-grained numerical-visual alignment.

Patch-wise Captioning. For numerical-text alignment, prior studies rely on time-series-agnostic texts, e.g., task prompts (Hu et al., 2025), external contexts (Zhang et al., 2025b), general word embeddings (Jin et al., 2024), which fail to capture nuanced physical variations of time series (e.g., amplitude, frequency), restricting semantic fidelity. We instead construct patch-wise captions grounded in numerical values. For each numerical patch $\mathbf{P}_{i;j}^n$, a structured caption $s_{i;j}$ consists of timestamp ranges and value statistics (e.g., max, min, mean, standard deviation), yielding a set of patch-wise captions $S_i = \{s_{i;1}, \dots, s_{i;\tilde{T}_i}\}$.

4.1.2. MULTI-MODAL ENCODING

Given expanded multi-modal inputs $\{\mathbf{x}_i, \mathbf{I}_i, S_i\}_{i=1}^{|\mathcal{X}|}$, numerical, visual, and textual modalities are encoded independently into continuous patch-level embeddings. Each instance is processed independently to accommodate variable sequence

lengths, while cross-instance dependencies are captured implicitly by the backbone LLM.

Numerical Encoding. We adopt a lightweight time series encoder consisting of linear projection, positional embedding, and transformer blocks:

$$\begin{aligned} \mathbf{P}_i^n &= [\mathbf{p}_{i;1}^n, \dots, \mathbf{p}_{i;\tilde{T}_i}^n]^\top = \text{Patching}(\mathbf{x}_i) \in \mathbb{R}^{\tilde{T}_i \times p^n}, \\ \mathbf{B}_i^n &= \text{LinearBlocks}(\text{Concat}(\mathbf{P}_i^n, \text{PosEmbed}(\mathbf{P}_i^n))), \quad (1) \\ \mathbf{E}_i^n &= \text{TransformerBlocks}(\mathbf{B}_i^n) \in \mathbb{R}^{\tilde{T}_i \times D}. \end{aligned}$$

Visual Encoding. The time series line plot is processed by the pre-trained vision encoder of the backbone MLLM: $\mathbf{E}_i^v = [\mathbf{e}_{i;1}^v, \dots, \mathbf{e}_{i;\tilde{T}_i}^v]^\top = \text{VisionEncoder}(\mathbf{I}_i) \in \mathbb{R}^{\tilde{T}_i \times D}$.

Caption Encoding. To encode the patch-wise caption $s_{i;j}$, we reuse the tokenizer and the input embedding layer of the backbone LLM. Then a mean pooling layer is applied to obtain patch-specific caption embeddings. This process is formulated as $\mathbf{e}_{i;j}^s = \text{MeanPool}(\text{LLM-Embed}(s_{i;j}))$, and $\mathbf{E}_i^s = [\mathbf{e}_{i;1}^s, \dots, \mathbf{e}_{i;\tilde{T}_i}^s]^\top \in \mathbb{R}^{\tilde{T}_i \times D}$ is the stacked tensor.

4.1.3. CONTRASTIVE ALIGNMENT

To strengthen semantic correspondence across modalities, we adopt a patch-wise contrastive learning objective. Numerical patch embeddings serve as anchors, while patch-aligned visual and textual caption embeddings are positives; all other patches within the same instance act as negatives. The *numerical-visual* alignment loss is defined with an InfoNCE objective (Oord et al., 2018):

$$\mathcal{L}_{\text{align}}^{n-v} = - \sum_{i,j} \log \frac{\exp(\text{sim}(\mathbf{e}_{i;j}^n, \text{sg}(\mathbf{e}_{i;j}^v))/\tau)}{\sum_{j'} \exp(\text{sim}(\mathbf{e}_{i;j}^n, \text{sg}(\mathbf{e}_{i;j'}^v))/\tau)}, \quad (2)$$

where sim denotes cosine similarity, sg denotes the stop-gradient operator, τ is a temperature parameter, and (i, j')

indexes all visual tokens within the i -th time series instance. The *numerical–caption* alignment loss $\mathcal{L}_{\text{align}}^{n-s}$ is computed analogously. We stop the gradients of encoded visual and textual tokens to optimize the numerical encoder only. The overall alignment objective is: $\mathcal{L}_{\text{PA}} = \mathcal{L}_{\text{align}}^{n-v} + \mathcal{L}_{\text{align}}^{n-s}$.

4.2. Discrete Disentangled Interaction

Building upon the aligned features, effective TSUR requires consolidating complementary semantics from numerical and visual modalities. We propose a *Discrete Disentangled Interaction (DDI)* module that performs modality disentanglement in a discrete latent space to enforce compact, consistent representations, and then integrates the isolated cross-modal unique signals. DDI consists of two stages: (1) *discrete modality disentanglement*, which extracts compact modality-common semantics via hierarchical vector quantization and derives modality-unique signals by residual decomposition; and (2) *unique-centric interaction*, which synergizes the unique signals via cross-attention.

4.2.1. DISCRETE MODALITY DISENTANGLEMENT

A straightforward approach to identify modality-unique semantics is to apply conventional disentanglement techniques (Qian et al., 2025), which use separate projection heads to extract modality-common and modality-specific representations, alongside regularization encouraging high correlation among common components and low correlation with unique components. However, existing methods (Xia et al., 2023; Huang et al., 2025) operate in continuous embedding spaces, which are unbounded and prone to capturing redundant or noisy correlations. In contrast, we perform disentanglement in a *discrete latent space* using vector quantization (VQ), which enforces compactness and consistency for modality-common semantics. Given numerical and visual tokens $\mathbf{E}_i^n, \mathbf{E}_i^v \in \mathbb{R}^{\tilde{T}_i \times D}$, we employ a shared hierarchical discretization block to extract modality-common representations \mathbf{Z}_i^n and \mathbf{Z}_i^v . The modality-unique components are then obtained by residual decomposition:

$$\mathbf{U}_i^n = \mathbf{E}_i^n - \mathbf{Z}_i^n, \quad \mathbf{U}_i^v = \mathbf{E}_i^v - \mathbf{Z}_i^v. \quad (3)$$

Hierarchical Discretization. To capture the multi-scale time series semantics, we propose a hierarchical RVQ strategy featured by M hierarchical codebooks $\{\mathcal{C}^{(m)}\}_{m=1}^M$, where the m -th codebook $\mathcal{C}^{(m)}$ contains $K \cdot 2^{m-1}$ codes and operates at a temporal resolution downsampled by 2^{M-m} tokens. Specifically, we first follow (Yu et al., 2022) and project continuous tokens $\mathbf{E}_i^n \in \mathbb{R}^{\tilde{T}_i \times D}$ to a lower-dimensional space via $\tilde{\mathbf{E}}_i^n = \text{Linear}(\mathbf{E}_i^n) \in \mathbb{R}^{\tilde{T}_i \times d}$, which increases the density of codes and reduces the quantization error. At each quantization stage m , given the residual token sequence $\mathbf{R}_i^{n;(m-1)} = [\mathbf{r}_{i;1}^{n;(m-1)}, \dots, \mathbf{r}_{i;\tilde{T}_i}^{n;(m-1)}]^\top \in \mathbb{R}^{\tilde{T}_i \times d}$ from the last round, we partition it into non-overlapping segments of length $W = 2^{M-m}$, and compute segment-level representations by average pooling over the tokens within each segment. These pooled representations are then broadcasted back to all token positions in the corresponding segment. This process can be formulated as $\tilde{\mathbf{r}}_{i;j}^{n;(m-1)} = \frac{1}{W} \sum_{b=j^*}^{j^*+W} \mathbf{r}_{i;b}^{n;(m-1)}$, where $j^* = [(j-1)/W]$ denotes the segment index of the j -th token. Afterwards, we follow the steps illustrated in Section 3.2, iteratively quantizing the residual features, from coarse to fine scales:

$$\begin{aligned} \mathbf{q}_{i;j}^{n;(m)} &= \arg \min_{\mathbf{c} \in \mathcal{C}^{(m)}} \|\tilde{\mathbf{r}}_{i;j}^{n;(m-1)} - \mathbf{c}\|_2^2, \\ \mathbf{r}_{i;j}^{n;(m)} &= \mathbf{r}_{i;j}^{n;(m-1)} - \mathbf{q}_{i;j}^{n;(m)}, \end{aligned} \quad (4)$$

where the initial residual tokens are $\mathbf{R}_i^{n;(0)} = \tilde{\mathbf{E}}_i^n$. The final discretized features are accumulated by $\mathbf{q}_{i;j}^n = \sum_{m=1}^M \mathbf{q}_{i;j}^{n;(m)}$. After quantization, the discrete representations should be projected back to D -dimensional space via $\mathbf{z}_{i;j}^n = \text{Linear}(\mathbf{q}_{i;j}^n) \in \mathbb{R}^D$, which serve as the modality-common tokens, and constitute $\mathbf{Z}_i^n \in \mathbb{R}^{\tilde{T}_i \times d}$. The modality-common tokens of visual time series \mathbf{Z}_i^v are derived in a similar way. The quantization process is supervised the \mathcal{L}_{vq} illustrated in Section 3.2.

Disentanglement Regularization. To effectively decouple modality-common and modality-unique information, we introduce two regularization terms. First, to align modality-common semantics, we apply a bidirectional contrastive objective between quantized numerical and visual tokens: $\mathcal{L}_{\text{com}} = \frac{1}{2}(\mathcal{L}_{\text{com}}^{n-v} + \mathcal{L}_{\text{com}}^{v-n})$, where

$$\mathcal{L}_{\text{com}}^{n-v} = - \sum_{i,j} \log \frac{\exp(\text{sim}(\mathbf{z}_{i;j}^n, \mathbf{z}_{i;j}^v)/\tau)}{\sum_{j'} \exp(\text{sim}(\mathbf{z}_{i;j}^n, \mathbf{z}_{i;j'}^v)/\tau)}. \quad (5)$$

To suppress leakage of shared semantics into modality-unique components, we enforce orthogonality between the common and unique tokens:

$$\mathcal{L}_{\text{orth}} = \frac{1}{2} \sum_{i,j} (|\text{sim}(\mathbf{z}_{i;j}^n, \mathbf{u}_{i;j}^n)| + |\text{sim}(\mathbf{z}_{i;j}^v, \mathbf{u}_{i;j}^v)|). \quad (6)$$

The overall objective for DDI is: $\mathcal{L}_{\text{DDI}} = \mathcal{L}_{\text{vq}} + \alpha \cdot \mathcal{L}_{\text{com}} + \beta \cdot \mathcal{L}_{\text{orth}}$, where α, β control the regularization strengths.

4.2.2. UNIQUE-CENTRIC INTERACTION

After disentanglement, modality-unique semantics are integrated via cross-modal attention. Each modality’s original tokens are augmented by attending to the unique signals (derived by Equation (3)) from the opposite modality:

$$\tilde{\mathbf{E}}_i^n = \mathbf{E}_i^n + \text{CrossAttn}(\mathbf{E}_i^n, \mathbf{U}_i^v, \mathbf{U}_i^v), \quad (7)$$

$$\tilde{\mathbf{E}}_i^v = \mathbf{E}_i^v + \text{CrossAttn}(\mathbf{E}_i^v, \mathbf{U}_i^n, \mathbf{U}_i^n). \quad (8)$$

This design enables fine-grained numerical dynamics and high-level visual patterns to complement each other.

4.3. Critical-token Highlighting

Although PA and DDI yield aligned and complementary representations, directly feeding them into the LLM may dilute question-relevant or inherently important information, limiting generalization. We propose a *Critical-token Highlighting (CTH)* module, which retains all original tokens and prepends several informative tokens to explicitly emphasize key signals, conditioned on both the question-aware and modality-intrinsic saliency. Specifically, the question Q is first tokenized and embedded as $\mathbf{E}^q = \text{LLM-Embed}(Q) \in \mathbb{R}^{N^q \times D}$. Given question embeddings \mathbf{E}^q , and continuous numerical/visual tokens $\mathbf{E}_i^o \in \mathbb{R}^{\tilde{T}_i \times D}$ ($o \in \{n, v\}$), CTH employs two parallel cross-attention branches.

Question-conditioned Branch. We first compress the variable-length question tokens into H learnable query tokens $\mathbf{Q}^q \in \mathbb{R}^{H \times D}$ via an attention-based pooling layer, and then use the compressed question-aware queries to attend over the modality tokens, which can be formulated as:

$$\begin{aligned} \tilde{\mathbf{Q}}^q &= \text{CrossAttn}(\mathbf{Q}^q, \mathbf{E}^q, \mathbf{E}^q), \\ \mathbf{H}_i^{o;q} &= \text{CrossAttn}(\tilde{\mathbf{Q}}^q, \mathbf{E}_i^o, \mathbf{E}_i^o), \quad o \in \{n, v\}. \end{aligned} \quad (9)$$

Modality-intrinsic Branch. In parallel, we introduce another set of H learnable queries $\mathbf{Q}^o \in \mathbb{R}^{H \times D}$ to identify modality-intrinsic patterns:

$$\mathbf{H}_i^{o;s} = \text{CrossAttn}(\mathbf{Q}^o, \mathbf{E}_i^o, \mathbf{E}_i^o), \quad o \in \{n, v\}. \quad (10)$$

The highlighted tokens are fused as $\mathbf{H}_i^o = \mathbf{H}_i^{o;q} + \mathbf{H}_i^{o;s}$ and prepended to the modality token sequence via $\hat{\mathbf{E}}_i^o = \text{Concat}(\mathbf{H}_i^o, \bar{\mathbf{E}}_i^o) \in \mathbb{R}^{(H+\tilde{T}_i) \times D}$, $o \in \{n, v\}$. This results in holistic and question-aware modality representations for LLM understanding and reasoning.

4.4. LLM Backbone and Training Objective

The enhanced numerical and visual tokens $\{\hat{\mathbf{E}}_i^n, \hat{\mathbf{E}}_i^v\}_{i=1}^{|\mathcal{X}|}$ are concatenated with textual input tokens, including the question tokens \mathbf{E}^q and context tokens \mathbf{E}^c (derived from the context C using the LLM's embeddings), via a position-aware concatenation operator (Xie et al., 2025):

$$\mathbf{E}^* = \text{PosConcat}(\mathbf{E}^c, \mathbf{E}^q, \{\hat{\mathbf{E}}_i^n, \hat{\mathbf{E}}_i^v\}_{i=1}^{|\mathcal{X}|}), \quad (11)$$

where $\text{PosConcat}(\cdot)$ integrates multi-modal tokens with the question tokens according to the positions of the time series instances in the original input. The fused sequence \mathbf{E}^* is fed into the backbone LLM to generate the answer A autoregressively: $P(A \mid \mathbf{E}^*) = \prod_{b=1}^{|A|} P(A_b \mid A_{<b}, \mathbf{E}^*)$, where A_b denotes the b -th token of the target answer sequence. In this study, we adopt Qwen2.5-VL-7B-Instruct (Bai et al., 2025) as our backbone MLLM. For model training, the language modeling loss is: $\mathcal{L}_{\text{LM}} = -\sum_{b=1}^{|A|} \log P(A_b \mid A_{<b}, \mathbf{E}^*)$,

and the overall training objective incorporates the regularization terms from PA and DDI: $\mathcal{L} = \mathcal{L}_{\text{LM}} + \lambda_1 \cdot \mathcal{L}_{\text{PA}} + \lambda_2 \cdot \mathcal{L}_{\text{DDI}}$, where λ_1, λ_2 denote the loss weights.

5. Experiment

5.1. Experimental Setups

Dataset. We use the training and evaluation data released with ChatTS (Xie et al., 2025), consisting of synthetic language-time series pairs for training and a hybrid of synthetic and real-world set for evaluation. The evaluation covers two types of tasks: (1) *Understanding tasks* assess fundamental characteristics of uni- or multi-variate time series, including noise, local fluctuation, seasonality, trend, as well as correlation and clustering patterns across variables; (2) *Reasoning tasks* involve inductive, deductive, causal, and comparison reasoning questions. Understanding tasks may require categorical choices or numerical calculations, whereas reasoning tasks mainly involve categorical questions, with some open-ended questions for inductive reasoning. Detailed descriptions of the datasets are provided in Appendix B.1.

Baseline. We compare our model against three types of baselines, grouped by the formulation of time series modalities: (1) *Numerical-centric models* directly process time series values, including general LLMs (GPT-4o (Hurst et al., 2024), Qwen3 (Yang et al., 2025), DeepSeek-V3.2 (Liu et al., 2025a), Gemini 3 Pro (Google, 2025), GPT-5.2 (OpenAI, 2025)) and time series-specific MLLMs (ChatTime (Wang et al., 2025a), ChatTS (Xie et al., 2025), ITFormer (Wang et al., 2025b), InstructTime (Cheng et al., 2025)); (2) *Visual-centric models* leverage time series plots (GPT-4o, Qwen3-VL (Shuai et al., 2025), Gemini 3 Pro, GPT-5.2); and (3) *Numerical+Visual models* integrate both modalities (GPT-4o, Qwen3-VL, Gemini 3 Pro, GPT-5.2, GEM (Lan et al., 2025)). General-purpose LLMs/MLLMs are accessed via APIs, while time-series-specialized MLLMs are fine-tuned on unified LLM backbones and training data. More details are provided in Appendix B.2.

Evaluation Metric. For categorical questions, we report *Accuracy* or *F1-Score*; for numerical questions, we use *Relative Accuracy* (Xie et al., 2025). For open-ended reasoning questions, we adopt *Answer Correctness* (Es et al., 2024), which measures the extent to which the model response covers the minimal set of essential facts (extracted by GPT-4o-mini (OpenAI, 2024)) required to answer the question.

The implementation details are provided in Appendix B.4.

5.2. Comparison Results

Table 1 reports performance on understanding tasks across synthetic and real-world datasets, while Table 2 summarizes results of reasoning tasks on the hybrid dataset. From

Table 1. Performance (%) on understanding tasks. The light-blue background denotes results from general-purpose LLMs/MLLMs accessed via APIs, while the light-red background denotes results from time-series-specific MLLMs.

Dataset	Type	Model	Noise		Local		Season		Trend		Corr.	Clus.	Overall	
			cate.	num.	cate.	num.	cate.	num.	cate.	num.	cate.	cate.	cate.	cate.
Synthetic	Numerical	DeepSeek-V3.2	74.39	47.15	31.70	23.13	78.35	67.16	78.57	85.04	36.64	30.20	43.81	37.74
		GPT-4o	56.10	43.21	14.77	9.72	88.66	55.16	72.62	83.80	34.81	30.09	38.36	26.81
		Qwen3	63.41	40.64	24.23	15.69	85.57	51.25	66.67	83.48	30.11	29.36	39.01	30.67
		GPT-5.2	73.17	43.03	41.41	34.88	96.91	72.09	78.57	93.01	47.20	37.27	52.27	47.88
		Gemini 3 Pro	84.15	59.67	53.12	45.82	95.88	84.10	76.19	83.26	54.12	49.16	60.48	55.63
		ChatTime	84.15	13.74	67.14	35.49	95.88	49.08	91.67	12.65	71.95	69.84	74.94	32.21
		ChatTS	93.90	47.20	84.38	76.02	100.00	86.64	96.43	96.34	81.07	79.27	85.32	79.54
		ITFormer	85.37	23.32	20.69	13.71	71.13	26.92	70.24	94.19	56.66	47.50	50.32	28.59
		InstructTime	79.27	19.34	22.32	15.24	70.10	11.23	72.62	96.27	52.29	48.06	49.34	28.60
	Visual	GPT-4o	64.63	31.72	34.39	26.97	87.63	65.01	50.00	48.23	39.54	43.90	46.59	33.79
	Visual	Qwen3-VL	53.66	18.92	34.37	26.31	90.72	49.71	80.95	49.08	38.81	41.70	47.71	31.92
	Visual	GPT-5.2	75.61	66.64	52.28	44.12	96.91	74.54	78.57	84.61	61.03	52.49	62.55	54.07
	Visual	Gemini 3 Pro	91.46	60.52	53.84	46.49	94.85	89.58	80.95	79.89	65.39	55.38	66.01	56.06
	Num.+Visual	GPT-4o	58.54	40.02	24.60	19.20	93.81	69.00	46.43	82.19	33.72	37.38	40.89	34.41
		Qwen3-VL	48.78	27.21	23.41	18.34	86.60	54.67	83.33	70.71	36.64	36.91	42.73	30.40
		GPT-5.2	73.17	61.05	43.25	36.42	98.97	79.38	75.00	93.61	59.21	48.32	58.58	50.27
		Gemini 3 Pro	86.59	70.51	53.92	46.88	97.94	86.52	76.19	83.88	63.57	54.72	64.90	56.96
		GEM	96.34	56.25	80.81	70.08	100.00	85.01	91.67	95.77	82.15	78.45	84.36	75.27
		MADI	98.78	78.39	91.45	84.73	100.00	93.27	94.05	96.60	86.89	84.35	89.99	87.22
Real-world	Numerical	DeepSeek-V3.2	85.71	29.30	60.72	46.14	81.08	0.00	65.85	88.09	61.11	51.73	63.86	50.35
		GPT-4o	95.24	19.97	32.15	24.16	78.38	0.00	70.73	84.49	57.03	46.12	54.80	34.86
		Qwen3	78.57	37.44	46.78	29.73	56.76	49.22	56.10	81.31	76.67	44.31	55.54	40.49
		GPT-5.2	92.86	31.88	57.86	45.06	97.30	0.00	60.98	96.02	81.11	56.90	69.47	52.33
		Gemini 3 Pro	92.86	24.76	86.07	72.08	91.89	70.27	56.10	81.16	84.08	76.88	80.25	67.36
		ChatTime	50.00	2.92	83.21	48.55	86.49	43.71	97.56	5.97	85.56	54.51	75.36	34.75
		ChatTS	88.10	47.09	86.78	78.40	97.30	84.60	92.68	90.01	68.52	62.94	82.39	77.01
		ITFormer	69.05	19.85	40.12	28.63	78.38	44.59	70.73	90.84	43.70	40.58	52.04	38.74
		InstructTime	54.76	11.22	32.73	24.67	97.30	0.00	75.61	96.04	52.59	30.89	51.53	36.16
	Visual	GPT-4o	97.62	20.10	64.41	53.05	94.59	0.00	34.15	68.48	55.18	62.75	64.22	50.17
	Visual	Qwen3-VL	97.62	30.93	63.81	50.41	59.46	20.54	80.49	53.75	54.45	61.80	66.97	47.60
	Visual	GPT-5.2	95.24	43.38	83.21	71.77	97.30	0.00	65.85	90.66	87.78	75.43	82.33	70.39
	Visual	Gemini 3 Pro	97.62	43.27	86.31	73.28	97.30	30.28	75.61	90.42	92.96	81.23	86.58	71.95
	Num.+Visual	GPT-4o	95.24	28.12	44.65	36.79	91.89	0.00	34.15	86.28	60.37	51.24	56.00	43.63
		Qwen3-VL	95.24	29.21	40.35	30.80	72.97	42.70	80.49	67.15	66.29	48.39	59.97	37.30
		GPT-5.2	88.10	43.86	82.98	71.40	97.30	0.00	65.85	96.14	87.41	68.44	79.44	71.03
		Gemini 3 Pro	97.62	46.32	86.31	72.76	97.30	68.75	63.41	82.95	92.96	82.47	85.18	70.99
	Num.+Visual	GEM	90.48	45.76	90.48	80.30	94.59	78.10	87.80	92.06	70.00	70.43	84.04	78.29
	Num.+Visual	MADI	97.62	55.95	93.81	86.30	100.00	94.42	87.80	88.48	77.78	70.14	88.54	83.78

these results, we draw the following key observations: (1) *MADI demonstrates strong and consistent understanding/reasoning capabilities*. It achieves clear improvements across both understanding and reasoning tasks, indicating that carefully designed multi-modal alignment and interaction mechanisms are crucial for effective TSUR. (2) *Visual plots are generally more effective than numerical sequences*. Visual-centric models outperform numerical-centric counterparts in most settings. For example, GPT-4o achieves up to 17% higher categorical accuracy on real-world understanding tasks. (3) *Naively combining modalities is insufficient*. For general-purpose LLMs, multi-modal inputs slightly degrade performance relative to visual-centric models, revealing the deficiency of simple modality concatenation, and the need for structured, fine-grained multi-modal learning strategies. (4) *General-purpose LLMs generalize better to real-world scenarios*. While their performance on synthetic datasets is modest (categorical accuracy $\sim 66\%$), general-purpose LLMs achieve substantially higher scores on real-world time series. For example, visually augmented Gemini 3 Pro outperforms several time-series-specialized MLLMs, such as ChatTS and GEM, on categorical understanding. In

contrast, models fine-tuned on synthetic data often degrade on real-world benchmarks, particularly in queries about cross-variable correlation and clustering. While this gap is partially attributable to model scale, it also reflects the challenge of robust real-world generalization in TSUR. (5) *Reasoning tasks are significantly harder than understanding tasks*. Performance on reasoning tasks is substantially lower than that on understanding tasks, emphasizing the intrinsic difficulty of higher-level time series reasoning and motivating further research in this direction. In addition, a computational cost analysis is provided in Appendix C, and detailed case studies are presented in Appendix D.

5.3. Ablation Study

We assess the contribution of individual components by comparing MADI with several ablated variants. “w/o PA”, “w/o DDI”, and “w/o CTH” remove the PA, DDI, and CTH modules, respectively. To evaluate fine-grained alignment and disentanglement, “w/o NVA” removes numerical-visual alignment, “w/o NCA” removes numerical-caption alignment, and “w/o MD” eliminates modality disentanglement.

Table 2. Performance (%) on reasoning tasks.

Type	Model	Induct.	Deduct.	Causal	MCQ2	Overall
Numerical	DeepSeek-V3.2	33.66	69.77	72.83	56.00	40.99
	GPT-4o	32.07	60.47	66.30	49.00	38.22
	Qwen3	32.38	48.84	68.48	46.00	37.93
	GPT-5.2	30.32	0.00	73.91	43.00	34.23
	Gemini 3 Pro	34.46	46.51	63.04	68.00	40.90
	ChatTime	49.18	48.84	53.26	44.00	49.07
	ChatTS	55.66	51.16	58.70	53.00	55.50
	ITFormer	42.54	44.19	47.83	46.00	43.48
	InstructTime	47.02	53.49	50.00	52.00	48.25
Visual	GPT-4o	28.86	62.79	68.48	51.00	36.03
	Qwen3-VL	33.11	51.16	60.87	55.00	38.75
	GPT-5.2	32.09	51.16	67.39	51.00	37.93
	Gemini 3 Pro	36.57	62.79	70.65	68.00	43.87
Num.+Visual	GPT-4o	26.81	55.81	69.57	47.00	33.93
	Qwen3-VL	29.70	51.16	69.57	54.00	36.76
	GPT-5.2	29.93	34.88	75.00	46.00	35.74
	Gemini 3 Pro	30.12	53.49	58.70	69.00	37.49
	GEM	58.73	67.44	66.30	53.00	59.30
	MADI	57.68	67.44	76.09	62.00	61.98

Furthermore, “w/o VQ” replaces hierarchical discretization in DDI with modality-shared continuous encoders, and “w/o Num.” removes the numerical modality, disabling PA and DDI. Figure 3 reports performance on categorical and numerical understanding, as well as reasoning tasks, revealing: (1) Alignment and interaction between different modalities are essential, as removing PA or DDI leads to substantial performance drops. (2) Highlighting critical, question-relevant information improves robustness and generalization, particularly for unseen reasoning tasks (“w/o CTH”). (3) Both numerical-visual and numerical-caption alignments are critical, as the performance gap between “w/o NVA”, “w/o NCA”, and the full model indicates a synergistic effect when both are employed. (4) Modality disentanglement (“w/o MD”) plays a pivotal role, as isolated unique signals significantly facilitate cross-modal interaction. (5) VQ is crucial for effective modality disentanglement and interaction, shown by the decrease in “w/o VQ”. (6) Numerical information contributes to robustness and generalization, but its benefits depend on well-designed multi-modal alignment and interaction (“w/o Num.” vs. full model).

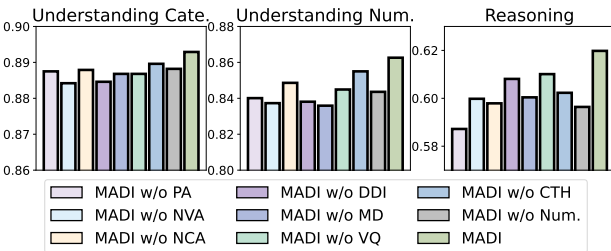


Figure 3. Ablation results of MADI.

5.4. Visualized Analysis

In this section, we empirically evaluate MADI’s ability to address the two key challenges identified in Section 1.

Alignment Analysis. To verify the effectiveness of fine-grained cross-modal grounding, we visualize the patch-wise cosine similarity matrices between numerical embeddings

and their visual/textual counterparts in Figure 4. Compared to the ablated variant (w/o PA), MADI exhibits clear diagonal high-similarity patterns, particularly between numerical and visual tokens. This confirms that the PA module successfully enforces precise patch-level correspondence across modalities. We further observe that the numerical-caption alignment is relatively less pronounced than the numerical-visual one, attributable to the semantic redundancy introduced by template-based caption generation, which makes patch-to-text consistency inherently more ambiguous.

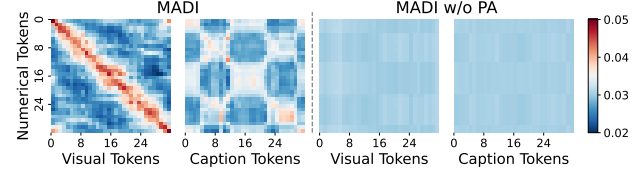


Figure 4. Heatmaps of cross-modal patch embedding similarities.

Disentanglement Analysis. To assess the quality of semantic decoupling in the DDI module, we analyze the kernel density estimation (KDE) distribution of cross-modal cosine similarities in Figure 5. We compare the similarity distributions of original continuous embeddings (*Continuous-Continuous*), disentangled modality-common signals (*Common-Common*), and modality-unique residuals (*Unique-Unique*). The results show that modality-common pairs exhibit higher similarity than their continuous counterparts, indicating successful concentration of shared semantics. In contrast, modality-unique pairs display substantially reduced correlation, verifying that DDI effectively isolates unique information from the shared subspace.

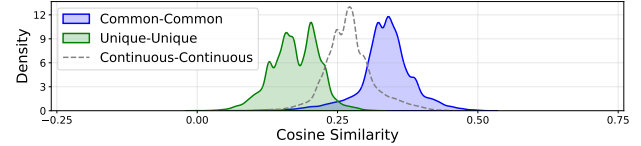


Figure 5. Distributions of cross-modal embedding similarities.

6. Conclusion

We present MADI, a multi-modal LLM for TSUR tasks that addresses the challenges of fine-grained alignment and disentangled interaction between numerical and visual modalities. The PA module enforces physically grounded correspondence across numerical, visual, and textual tokens, while the DDI module separates modality-common and modality-specific semantics to synergistically fuse complementary signals. The CTH module further emphasizes informative, query-relevant tokens to enhance reasoning robustness. Extensive experiments on synthetic and real-world benchmarks demonstrate that MADI consistently outperforms general-purpose LLMs and time-series-specialized MLLMs, validating the effectiveness of structured multi-modal integration and highlighting its potential to advance interpretable and flexible time series analysis.

Impact Statement

This work aims to advance the field of machine learning by developing a numerical-visual MLLM, MADI, for interpretable and flexible time series understanding and reasoning. By effectively integrating numerical precision and visual abstraction, MADI enhances the ability of AI systems to analyze temporal data across diverse domains such as healthcare, finance, climate, and infrastructure monitoring. While the model is designed for general-purpose time series analysis, we recognize that its deployment in sensitive real-world applications, such as medical diagnosis, financial forecasting, or autonomous systems, requires careful consideration of data privacy, algorithmic fairness, and robustness to distribution shifts. We encourage future work to incorporate ethical safeguards, domain-specific validation, and human-in-the-loop oversight to mitigate potential risks associated with misinterpretation or over-reliance on automated decisions. Ultimately, we believe this research contributes to the development of more transparent, adaptable, and trustworthy AI tools for time-series analytics, with broadly beneficial societal implications.

References

- Bai, S., Chen, K., Liu, X., Wang, J., Ge, W., Song, S., Dang, K., Wang, P., Wang, S., Tang, J., et al. Qwen2.5-vl technical report. *arXiv preprint arXiv:2502.13923*, 2025.
- Chen, J., Feng, A., Zhao, Z., Garza, J., Nurbek, G., Qin, C., Maatouk, A., Tassiulas, L., Gao, Y., and Ying, R. Mtbench: A multimodal time series benchmark for temporal reasoning and question answering. *arXiv preprint arXiv:2503.16858*, 2025.
- Cheng, M., Chen, Y., Liu, Q., Liu, Z., Luo, Y., and Chen, E. Instructime: Advancing time series classification with multimodal language modeling. In *Proceedings of the Eighteenth ACM International Conference on Web Search and Data Mining*, 2025.
- Ding, K., Fan, F., Wang, Y., Jian, R., Wang, X., Gong, L., Jiang, Y., Luo, C., and Zhan, J. Dualsg: A dual-stream explicit semantic-guided multivariate time series forecasting framework. In *Proceedings of the 33rd ACM International Conference on Multimedia*, 2025.
- Dong, S., Fan, W., Wu, T., and Fu, Y. Teaching time series to see and speak: Forecasting with aligned visual and textual perspectives. *arXiv preprint arXiv:2506.24124*, 2025.
- Es, S., James, J., Anke, L. E., and Schockaert, S. Ragas: Automated evaluation of retrieval augmented generation. In *Proceedings of the 18th Conference of the European Chapter of the Association for Computational Linguistics: System Demonstrations*, 2024.
- Google. Gemini 3 pro. <https://deepmind.google/models/gemini/pro/>, 2025. Accessed 2025.
- Gruver, N., Finzi, M., Qiu, S., and Wilson, A. G. Large language models are zero-shot time series forecasters. In *Proceedings of the 37th International Conference on Neural Information Processing Systems*, 2023.
- Hu, Y., Li, Q., Zhang, D., Yan, J., and Chen, Y. Context-alignment: Activating and enhancing llms capabilities in time series. In *The Thirteenth International Conference on Learning Representations*, 2025.
- Huang, H., Xia, Y., Ji, S., Wang, S., Wang, H., Fang, M., Zhu, J., Dong, Z., Zhou, S., and Zhao, Z. Enhancing multimodal unified representations for cross modal generalization. In *Findings of the Association for Computational Linguistics: ACL 2025*, 2025.
- Hurst, A., Lerer, A., Goucher, A. P., Perelman, A., Ramesh, A., Clark, A., Ostrow, A., Welihinda, A., Hayes, A., Radford, A., et al. Gpt-4o system card. *arXiv preprint arXiv:2410.21276*, 2024.
- Jiang, Y., Yu, W., Lee, G., Song, D., Shin, K., Cheng, W., Liu, Y., and Chen, H. TimeXL: Explainable multi-modal time series prediction with llm-in-the-loop. In *Proceedings of the 39th International Conference on Neural Information Processing Systems*, 2025.
- Jin, M., Wang, S., Ma, L., Chu, Z., Zhang, J. Y., Shi, X., Chen, P.-Y., Liang, Y., Li, Y.-F., Pan, S., and Wen, Q. Time-llm: Time series forecasting by reprogramming large language models. In *The Twelfth International Conference on Learning Representations*, 2024.
- Lan, X., Wu, F., He, K., Zhao, Q., Hong, S., and Feng, M. Gem: Empowering mllm for grounded ecg understanding with time series and images. In *Proceedings of the 39th International Conference on Neural Information Processing Systems*, 2025.
- Lee, D., Kim, C., Kim, S., Cho, M., and Han, W.-S. Autoregressive image generation using residual quantization. In *Proceedings of the IEEE/CVF Conference on Computer Vision and Pattern Recognition*, 2022.
- Li, H., Jung, E., CHEN, Z., Wang, Z., WANG, Y., Qu, H., and Lau, A. K. H. Pipe: Physics-informed position encoding for alignment of satellite images and time series in typhoon forecasting. In *Proceedings of the 39th International Conference on Neural Information Processing Systems*, 2025.
- Liu, A., Mei, A., Lin, B., Xue, B., Wang, B., Xu, B., Wu, B., Zhang, B., Lin, C., Dong, C., et al. Deepseek-v3.2: Pushing the frontier of open large language models. *arXiv preprint arXiv:2512.02556*, 2025a.

- Liu, C., Xu, Q., Miao, H., Yang, S., Zhang, L., Long, C., Li, Z., and Zhao, R. Timecma: Towards llm-empowered multivariate time series forecasting via cross-modality alignment. In *Proceedings of the Thirty-Ninth AAAI Conference on Artificial Intelligence and Thirty-Seventh Conference on Innovative Applications of Artificial Intelligence and Fifteenth Symposium on Educational Advances in Artificial Intelligence*, 2025b.
- Liu, H., Xu, S., Zhao, Z., Kong, L., Kamarthi, H., Sasanur, A. B., Sharma, M., Cui, J., Wen, Q., Zhang, C., and Prakash, B. A. Time-mmd: Multi-domain multimodal dataset for time series analysis. In *Proceedings of the 38th International Conference on Neural Information Processing Systems*, 2024.
- Liu, H., Liu, C., and Prakash, B. A. A picture is worth a thousand numbers: Enabling llms reason about time series via visualization. In *Proceedings of the 2025 Conference of the Nations of the Americas Chapter of the Association for Computational Linguistics: Human Language Technologies*, 2025c.
- Liu, P., Guo, H., Dai, T., Li, N., Bao, J., Ren, X., Jiang, Y., and Xia, S.-T. Calf: Aligning llms for time series forecasting via cross-modal fine-tuning. In *Proceedings of the Thirty-Ninth AAAI Conference on Artificial Intelligence and Thirty-Seventh Conference on Innovative Applications of Artificial Intelligence and Fifteenth Symposium on Educational Advances in Artificial Intelligence*, 2025d.
- Merrill, M. A., Tan, M., Gupta, V., Hartvigsen, T., and Althoff, T. Language models still struggle to zero-shot reason about time series. In *Findings of the Association for Computational Linguistics: EMNLP 2024*, 2024.
- Nie, Y., Nguyen, N. H., Sinthong, P., and Kalagnanam, J. A time series is worth 64 words: Long-term forecasting with transformers. In *The Eleventh International Conference on Learning Representations*, 2023.
- Oord, A. v. d., Li, Y., and Vinyals, O. Representation learning with contrastive predictive coding. *arXiv preprint arXiv:1807.03748*, 2018.
- OpenAI. Gpt-4o mini. <https://platform.openai.com/docs/models/gpt-4o-mini>, 2024. Accessed 2025.
- OpenAI. Introducing gpt-5.2. <https://openai.com/index/introducing-gpt-5-2/>, 2025. Accessed 2025.
- Qian, C., Xing, S., Li, S., Zhao, Y., and Tu, Z. Decalign: Hierarchical cross-modal alignment for decoupled multimodal representation learning. *arXiv preprint arXiv:2503.11892*, 2025.
- Shuai, B., Yuxuan, C., Ruizhe, C., Kejin, C., Xionghui, C., Zesen, C., Lianghao, D., Wei, D., Chang, G., Chunjiang, G., et al. Qwen3-vl technical report. *arXiv preprint arXiv:2511.21631*, 2025.
- Tan, M., Merrill, M., Gupta, V., Althoff, T., and Hartvigsen, T. Are language models actually useful for time series forecasting? In *Proceedings of the 38th International Conference on Neural Information Processing Systems*, 2024.
- van den Oord, A., Vinyals, O., and Kavukcuoglu, K. Neural discrete representation learning. In *Proceedings of the 31st International Conference on Neural Information Processing Systems*, 2017.
- Wang, C., Qi, Q., Wang, J., Sun, H., Zhuang, Z., Wu, J., Zhang, L., and Liao, J. Chattime: A unified multimodal time series foundation model bridging numerical and textual data. In *Proceedings of the Thirty-Ninth AAAI Conference on Artificial Intelligence and Thirty-Seventh Conference on Innovative Applications of Artificial Intelligence and Fifteenth Symposium on Educational Advances in Artificial Intelligence*, 2025a.
- Wang, Y., Wu, H., Dong, J., Liu, Y., Wang, C., Long, M., and Wang, J. Deep time series models: A comprehensive survey and benchmark. *arXiv preprint arXiv:2407.13278*, 2024.
- Wang, Y., Lei, P., Song, J., Hao, Y., Chen, T., Zhang, Y., Jia, L., Li, Y., and Wei, Z. Itformer: Bridging time series and natural language for multi-modal qa with large-scale multitask dataset. In *Forty-second International Conference on Machine Learning*, 2025b.
- Xia, Y., Huang, H., Zhu, J., and Zhao, Z. Achieving cross modal generalization with multimodal unified representation. In *Proceedings of the 37th International Conference on Neural Information Processing Systems*, 2023.
- Xie, Z., Li, Z., He, X., Xu, L., Wen, X., Zhang, T., Chen, J., Shi, R., and Pei, D. Chatts: Aligning time series with llms via synthetic data for enhanced understanding and reasoning. *Proc. VLDB Endow.*, 2025.
- Xu, X., Wang, H., Liang, Y., Yu, P. S., Zhao, Y., and Shu, K. Can multimodal llms perform time series anomaly detection? *arXiv preprint arXiv:2502.17812*, 2025.
- Yang, A., Yang, B., Zhang, B., Hui, B., Zheng, B., Yu, B., Li, C., Liu, D., Huang, F., Wei, H., et al. Qwen2.5 technical report. *arXiv preprint arXiv:2412.15115*, 2024.
- Yang, A., Li, A., Yang, B., Zhang, B., Hui, B., Zheng, B., Yu, B., Gao, C., Huang, C., Lv, C., et al. Qwen3 technical report. *arXiv preprint arXiv:2505.09388*, 2025.

Yu, J., Li, X., Koh, J. Y., Zhang, H., Pang, R., Qin, J., Ku, A., Xu, Y., Baldridge, J., and Wu, Y. Vector-quantized image modeling with improved VQGAN. In *The Tenth International Conference on Learning Representations*, 2022.

Zhang, J., Feng, L., Guo, X., Wu, Y., Dong, Y., and Xu, D. Timemaster: Training time-series multimodal llms to reason via reinforcement learning. *arXiv preprint arXiv:2506.13705*, 2025a.

Zhang, Y., Yang, W., Wang, J., Ma, Q., and Xiong, J. Camef: Causal-augmented multi-modality event-driven financial forecasting by integrating time series patterns and salient macroeconomic announcements. In *Proceedings of the 31st ACM SIGKDD Conference on Knowledge Discovery and Data Mining V.2*, 2025b.

Zhao, Z., Shen, C., Tong, H., Song, D., Deng, Z., Wen, Q., and Ni, J. From images to signals: Are large vision models useful for time series analysis? *arXiv preprint arXiv:2505.24030*, 2025.

Zhong, S., Ruan, W., Jin, M., Li, H., Wen, Q., and Liang, Y. Time-vlm: Exploring multimodal vision-language models for augmented time series forecasting. In *Forty-second International Conference on Machine Learning*, 2025.

Zhou, S., Schöner, H., Lyu, H., Fouché, E., and Wang, S. Balm-tsf: Balanced multimodal alignment for llm-based time series forecasting. In *Proceedings of the 34th ACM International Conference on Information and Knowledge Management*, 2025.

A. Notation

The key notations used in this paper are summarized in Table 3.

Table 3. Summary of Notations.

Notation	Description
General & Problem Definition	
\mathcal{X}	Set of time series inputs, containing instances \mathbf{x}_i
\mathbf{x}_i	The i -th time series instance
T_i	Number of observations in time series \mathbf{x}_i
C, Q	Context and question textual inputs
$\mathbf{E}^c, \mathbf{E}^q$	Embeddings for context and question, composed of tokens $\mathbf{e}^c, \mathbf{e}^q$
A	Generated textual answer
Patch-level Alignment (PA)	
p^n	Patch size for numerical time series
p^v	Patch size for the vision encoder
\tilde{T}_i	Number of patches for \mathbf{x}_i
\mathbf{P}_i^n	Numerical time series patches, composed of $\mathbf{P}_{i;j}^n$
\mathbf{I}_i	Visualized line plot image
S_i	Set of patch-wise textual captions $\{s_{i;j}\}$
D	Embedding dimension of above encoders and the LLM backbone
\mathbf{E}_i^n	Encoded numerical embeddings, composed of tokens $\mathbf{e}_{i;j}^n$
\mathbf{E}_i^v	Encoded visual embeddings, composed of tokens $\mathbf{e}_{i;j}^v$
\mathbf{E}_i^s	Encoded caption embeddings, composed of tokens $\mathbf{e}_{i;j}^s$
Discrete Disentangled Interaction (DDI)	
$\mathbf{Z}_i^n, \mathbf{Z}_i^v$	Modality-common representations, composed of tokens $\mathbf{z}_{i;j}^n, \mathbf{z}_{i;j}^v$
$\mathbf{U}_i^n, \mathbf{U}_i^v$	Modality-unique representations, composed of tokens $\mathbf{u}_{i;j}^n, \mathbf{u}_{i;j}^v$
d	Reduced embedding dimension during vector quantization
$\mathcal{C}^{(m)}$	The m -th codebook in hierarchical vector quantization
$\mathbf{R}_i^{n;(m)}, \mathbf{R}_i^{v;(m)}$	Residuals at quantization stage m , composed of tokens $\mathbf{r}_{i;j}^{n;(m)}, \mathbf{r}_{i;j}^{v;(m)}$
$\tilde{\mathbf{R}}_i^{n;(m)}, \tilde{\mathbf{R}}_i^{v;(m)}$	Pooled and broadcasted residuals at stage m , composed of tokens $\tilde{\mathbf{r}}_{i;j}^{n;(m)}, \tilde{\mathbf{r}}_{i;j}^{v;(m)}$
$\mathbf{Q}_i^{n;(m)}, \mathbf{Q}_i^{v;(m)}$	Quantized discrete modality representations, composed of $\mathbf{q}_{i;j}^{n;(m)}, \mathbf{q}_{i;j}^{v;(m)}$
$\mathbf{E}_i^n, \mathbf{E}_i^v$	Augmented modality tensors after cross-modal interaction
Critical-token Highlighting (CTH)	
\mathbf{Q}^q	Learnable queries for the question-conditioned branch
$\mathbf{Q}^n, \mathbf{Q}^v$	Learnable queries for the modality-intrinsic branch
$\mathbf{H}_i^{n;q}, \mathbf{H}_i^{v;q}$	Highlighted tokens from the question-conditioned branch
$\mathbf{H}_i^{n;s}, \mathbf{H}_i^{v;s}$	Highlighted tokens from the modality-intrinsic branch
$\mathbf{H}_i^n, \mathbf{H}_i^v$	Highlighted tokens fused from question-conditioned and modality-intrinsic branches
$\hat{\mathbf{E}}_i^n, \hat{\mathbf{E}}_i^v$	Final enhanced modality embeddings prepended with highlighted tokens
\mathbf{E}^*	Final fused multi-modal sequence input to the LLM
Optimization Objectives & Hyperparameters	
\mathcal{L}_{PA}	Total Patch-level Alignment loss
$\mathcal{L}_{align}^{n-v}, \mathcal{L}_{align}^{n-s}$	Contrastive alignment losses for numerical-visual and numerical-caption pairs
\mathcal{L}_{DDI}	Total Discrete Disentangled Interaction loss
\mathcal{L}_{vq}	Vector quantization commitment loss
\mathcal{L}_{com}	Bidirectional contrastive loss for modality-common semantics
\mathcal{L}_{orth}	Orthogonality loss between common and unique components
\mathcal{L}_{LM}	Language modeling loss
τ	Temperature hyperparameter for contrastive learning
α, β	Weights for disentanglement regularization terms
λ_1, λ_2	Loss weights for PA and DDI modules

B. Experimental Details

B.1. Dataset

Our experiments utilize the datasets released by ChatTS (Xie et al., 2025), which are designed for time series understanding and reasoning (TSUR). The data are divided into training and evaluation sets and are sourced from both synthetic generation and real-world domains.

B.1.1. TRAINING DATA CONSTRUCTION

Due to the scarcity of high-quality, well-aligned time series–text pairs, the training data are primarily constructed via a synthetic generation pipeline (Xie et al., 2025) consisting of two key modules:

- **Attribute-Based Generation:** To ensure precise alignment between numerical values and textual descriptions, time series are generated from a predefined *Attribute Pool* covering four major categories: *Trend*, *Periodicity*, *Noise*, and *Local Fluctuations* (e.g., spikes and phase changes). An *Attribute Selector* samples attributes to construct time series arrays while simultaneously generating ground-truth textual descriptions based on the selected attributes.
- **Time Series Evol-Instruct (TSEvol):** To enhance data diversity and reasoning complexity, we adopt an evolutionary instruction generation strategy. Starting from seed question–answer pairs, an LLM progressively evolves questions into more complex forms, while querying the attribute pool to ensure factual consistency.

B.1.2. EVALUATION DATA COMPOSITION

The evaluation dataset is a hybrid of real-world and synthetic data, designed to assess out-of-distribution generalization. The synthetic samples are generated using the same pipeline described in Appendix B.1.1. The real-world data are collected from diverse domains, including AIOps (system monitoring metrics), weather (temperature and humidity), finance (stock trends), and traffic flow. All real-world samples are manually annotated by domain experts to ensure annotation accuracy.

Concretely, the evaluation dataset comprises two primary task categories:

- **Understanding Tasks:** These tasks evaluate the model’s ability to ground textual concepts in time series features. Subtasks include identifying *Trend* (increase/decrease), *Seasonality* (period length), *Noise Levels*, and *Local Fluctuations* (spike/dip detection). For multivariate time series, additional tasks include *Correlation* analysis and *Clustering*. Questions are presented in both categorical (multiple-choice) and numerical (value extraction) formats.
- **Reasoning Tasks:** These tasks assess higher-order reasoning capabilities. Subtasks include *Inductive Reasoning* (inferring physical meanings from patterns), *Deductive Reasoning* (predicting behavior under given conditions), *Causal Reasoning* (identifying root causes of anomalies), and *Comparison* (contrasting distinct time series). Questions are provided in categorical or open-ended formats.

B.2. Baselines

To ensure rigorous comparisons, we group baselines into general-purpose LLMs/MLLMs and specialized time series MLLMs.

General LLMs and MLLMs. We evaluate general-purpose models including GPT-4o (Hurst et al., 2024), Qwen3 (Yang et al., 2025), Qwen3-VL (Shuai et al., 2025), DeepSeek-V3.2 (Liu et al., 2025a), Gemini 3 Pro (Google, 2025), and GPT-5.2 (OpenAI, 2025), using their official APIs. Numerical-only LLMs receive time series in serialized numerical form, while visual-based MLLMs additionally receive time series rendered as images. Following (Xie et al., 2025), we visualize time series using line plots; for multivariate data, plots of different variables are stacked into a single composite figure.

Time-Series-Specialized MLLMs. For specialized baselines, including ChatTime (Wang et al., 2025a), ChatTS (Xie et al., 2025), ITFormer (Wang et al., 2025b), InstructTime (Cheng et al., 2025), and GEM (Lan et al., 2025), we unify the LLM backbone to ensure a fair comparison that emphasizes architectural design rather than base model capacity. All specialized models are reproduced and fine-tuned using either Qwen2.5-7B-Instruct (Yang et al., 2024) or Qwen2.5-VL-7B-Instruct (Bai et al., 2025) for numerical–visual multimodal settings. We strictly maintain identical training data and experimental environments across all baselines and our proposed MADI.

B.3. Evaluation Metrics

We adopt different evaluation metrics for categorical, numerical, and open-ended reasoning tasks.

Categorical Tasks. For classification-based questions (e.g., trend direction and fluctuation type), we report *Accuracy* and *F1-score*, measuring the agreement between predicted labels and ground truth.

Numerical Tasks. For tasks requiring numerical value estimation (e.g., spike amplitude or period length), we employ *Relative Accuracy* (Acc_{rel}) with thresholding to reduce sensitivity to outliers:

$$\text{Acc}_{\text{rel}} = \max \left(0, 1 - \left| \frac{v_{\text{pred}} - v_{\text{label}}}{v_{\text{label}}} \right| \right), \quad (12)$$

where v_{pred} denotes the value extracted from the model response and v_{label} is the ground-truth value.

Open-ended Reasoning Tasks. For open-ended reasoning tasks, we adopt the *Answer Correctness* metric from RAGAS framework (Es et al., 2024). This metric uses a judge LLM (GPT-4o-mini) to extract key facts from the ground-truth answer and computes the recall of these facts in the model response, enabling semantic evaluation beyond naive keyword matching.

B.4. Implementation Details

This section describes the implementation details of MADI, including data preprocessing, model hyperparameters, and training and evaluation configurations.

Statistics-Preserved Normalization. To improve training stability and reduce distribution shifts across heterogeneous time series domains, we apply zero-centered normalization to the input series prior to patch-level modality expansion. While normalization is essential for effective optimization, it removes absolute magnitude information that is crucial for precise numerical reasoning (e.g., answering queries such as “what is the maximum value?”).

To address this limitation, we introduce a *Statistics-Preserved Prompt* that explicitly encodes global statistics of the original time series and exposes them to the LLM during reasoning. Specifically, for each time series instance \mathbf{x}_i , we construct a structured textual prompt containing its normalization parameters (offset and scaling factor), sequence length, and key boundary statistics, including the maximum, minimum, start, and end values. This prompt is prepended to the processed multi-modal tokens $\hat{\mathbf{E}}_i^n$, enabling the LLM to recover the original scale and perform accurate value-based reasoning.

The statistics-preserved prompt follows the format:

$$[\text{offset}=\dots | \text{scaling}=\dots | \text{length}=\dots | \text{max}=\dots | \text{min}=\dots | \text{left}=\dots | \text{right}=\dots] \quad (13)$$

where:

- **offset**: the offset applied during normalization (e.g., the negative mean);
- **scaling**: the scaling factor used for normalization;
- **length**: the length of the time series sequence;
- **max / min**: the maximum and minimum values of the original series;
- **left / right**: the first and last values in the sequence.

By exposing these global statistics, MADI leverages the arithmetic reasoning capabilities of the LLM backbone to interpret normalized temporal patterns with respect to their original physical magnitudes. For consistency across modalities, visual plots and patch-level captions are also generated from the normalized series, ensuring alignment with the numerical inputs.

Model Hyperparameters. The embedding dimension is set to $D = 3584$ to match the LLM backbone. We use a numerical patch size of $p^n = 8$, a discretization dimension of $d = 512$, and $m = 3$ hierarchical codebook levels. The overall loss is a weighted sum of multiple components, with weights $\alpha = 5$ (modality-common alignment), $\beta = 1$ (common-unique orthogonalization), $\lambda_1 = 0.02$ (PA regularization), and $\lambda_2 = 0.2$ (DDI regularization).

Training Configuration. We implement our model and training pipeline using the LLaMA-Factory framework on 4× NVIDIA A800 GPUs. Specifically, we adopt a per-device batch size of 2 with 64 gradient accumulation steps, resulting in

an effective batch size of $512 = 4 \times 2 \times 64$. Optimization is performed using AdamW with a learning rate of 1×10^{-5} and a cosine learning rate scheduler, together with a warmup ratio of 0.02. Training proceeds for 1200 steps. We employ a two-stage training strategy: during the initial warmup phase (0.02 of total training), the LLM backbone and vision encoder (for Qwen2.5-VL-based models) are frozen, and only newly introduced modules are trained; afterward, all parameters are unfrozen for full fine-tuning.

Evaluation Configuration. During evaluation, we set the decoding temperature to 0.01 to ensure stable and reproducible results across all benchmarks. Evaluation is conducted every 50 steps, and the checkpoint with the best evaluation performance is selected for final reporting.

C. Token Cost Analysis

In this section, we evaluate the computational efficiency of different paradigms by calculating the average token consumption per query in real-world understanding tasks, as presented in Table 4. This reveals significant disparities driven by tokenization strategies and input modalities.

Table 4. Average token cost per query across different kinds of models.

Type	Numerical									
Model	DeepSeek	GPT-4o	Qwen3	GPT-5.2	Gemini	InstructTime	ITFormer	ChatTime	ChatTS	
Cost	7135.90	7140.04	9935.51	7139.04	9702.75	1108.16	1108.16	2503.01	1118.90	
Type	Visual									
Model	GPT-4o	Qwen3-VL	GPT-5.2	Gemini	GPT-4o	Qwen3-VL	GPT-5.2	Gemini	GEM	MADI
Cost	1063.49	1390.13	1111.86	1643.47	7698.82	10800.71	7864.87	10800.93	1174.99	1517.79

In the *Numerical-centric* setting, general-purpose LLMs (e.g., GPT-4o, DeepSeek) exhibit prohibitively high consumption, consistently exceeding 7,000 tokens per query. This inefficiency stems from their reliance on digit-level tokenization, where a single time-series value is decomposed into multiple tokens. Even time-series-specific adaptations like ChatTime, which utilizes value-level tokenization, incur a noticeably higher cost compared to patch-based models (e.g., ITFormer, ChatTS, MADI) that efficiently aggregate temporal segments into compact vector representations.

The computational burden is further exacerbated in the *Numerical+Visual* setting. For standard Multi-modal LLMs such as Qwen3-VL and GPT-4o, the straightforward concatenation of lengthy numerical text sequences with visual embeddings results in excessive sequence lengths, often surpassing 10,000 tokens. This significantly increases the inference overhead. In contrast, MADI incorporates rich multi-modal semantics with only a marginal increase in token count compared to the most efficient baselines. Consequently, MADI achieves the best performance trade-off, delivering robust reasoning capabilities with a modest token cost.

D. Case Study

In this section, we present qualitative case studies across a spectrum of time series understanding and reasoning tasks. These examples serve to empirically demonstrate the capabilities of MADI compared to three competitive baselines: Gemini 3 Pro (Visual-centric), ChatTS (Numerical-centric), and GEM (Numerical+Visual).

Noise Understanding. Figure 6 evaluates noise quantification using solar radiation data, a domain characterized by subtle, high-frequency fluctuations. Although baseline models, such as Gemini 3 Pro, fail to perceive these fine-grained perturbations—incorrectly classifying the series as noiseless, MADI exhibits superior sensitivity. It accurately detects the “noisy” nature of the signal and provides a precise standard deviation estimate of 0.05. This result underscores the model’s ability to distinguish inherent signal stochasticity from clean trends, a capability often lacking in existing methods.

Local Fluctuation Understanding. Figure 7 illustrates the challenge of characterizing morphological features within traffic signal data. The series exhibits complex local behaviors, specifically a rapid “shake” followed by a sharp decline. Baselines like Gemini 3 Pro and ChatTS oversimplify these patterns, hallucinating generic “convex” shapes or “upward spikes”. In contrast, MADI demonstrates high morphological fidelity, accurately localizing and classifying the “shake” at point 149 and the “decrease after downward spike” at point 185. This highlights the model’s precision in parsing fine-grained structural

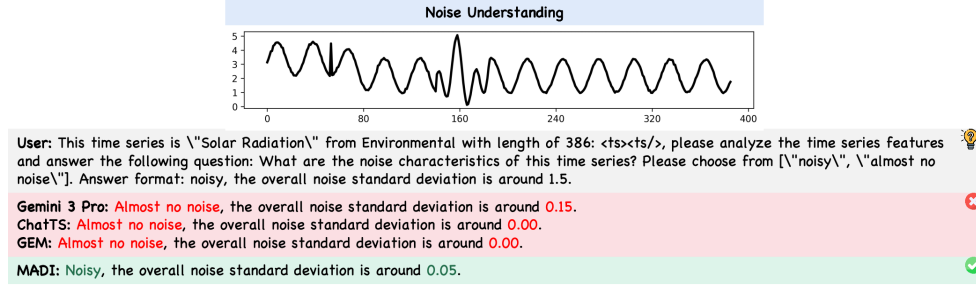


Figure 6. Case study of noise understanding.

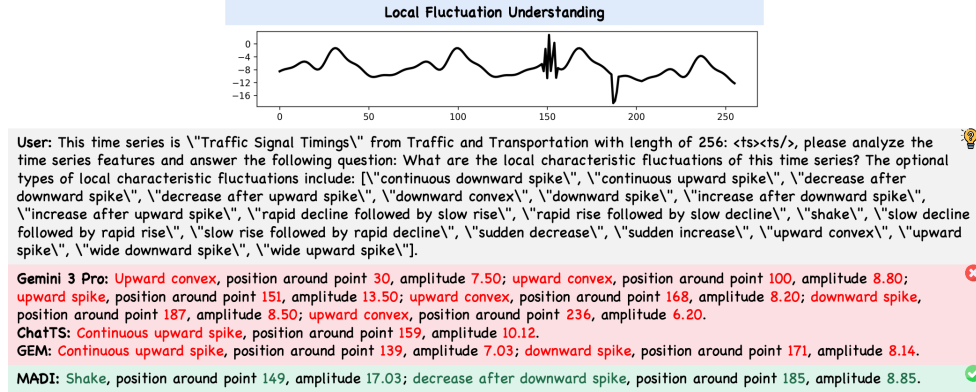


Figure 7. Case study of local fluctuation understanding.

changes in complicated temporal data.

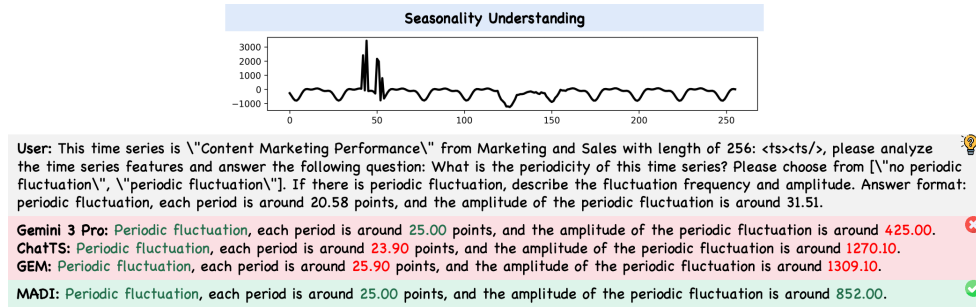


Figure 8. Case study of seasonality understanding.

Seasonality Understanding. Figure 8 examines seasonality extraction in content marketing performance data, where regular cycles are disrupted by a significant anomaly. This irregularity causes baselines to falter: ChatTS and GEM are sensitive to the outlier, resulting in a gross overestimation of amplitude, while Gemini 3 Pro underestimates it. MADI, however, proves robust to such contamination, correctly identifying the period (25.00) and providing a reliable amplitude estimate (852.00). This demonstrates the model’s capacity to identify true periodic features from sporadic irregularities.

Trend Understanding. Figure 9 depicts a trend analysis task on external service call latency data. The series is defined by high volatility and a late-stage downward shift. Although baselines like Gemini 3 Pro and GEM misinterpret the global behavior as strictly “Decreasing”, and ChatTS fail to capture the precise values of the starting point and global shift, MADI correctly identifies the overall “Steady” state while accurately quantifying the specific trend change value (-62.01). This validates the model’s ability to maintain a global perspective despite local volatility.

Correlation Understanding and Inductive Reasoning. Figure 10 presents a complex task requiring both correlation analysis and inductive reasoning on network “Jitter” and “Throughput” metrics. Baselines (e.g., Gemini 3 Pro, ChatTS)

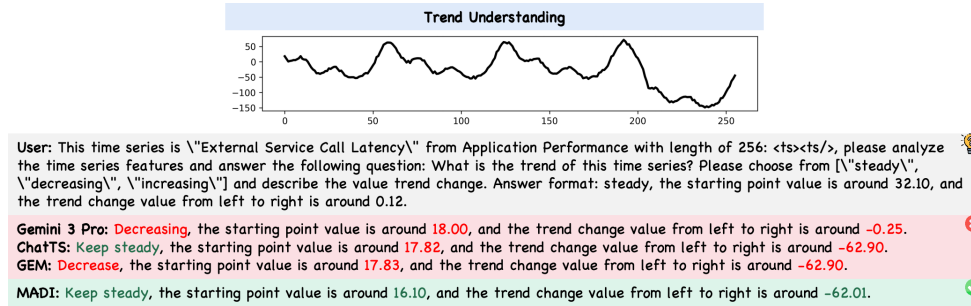


Figure 9. Case study of trend understanding.

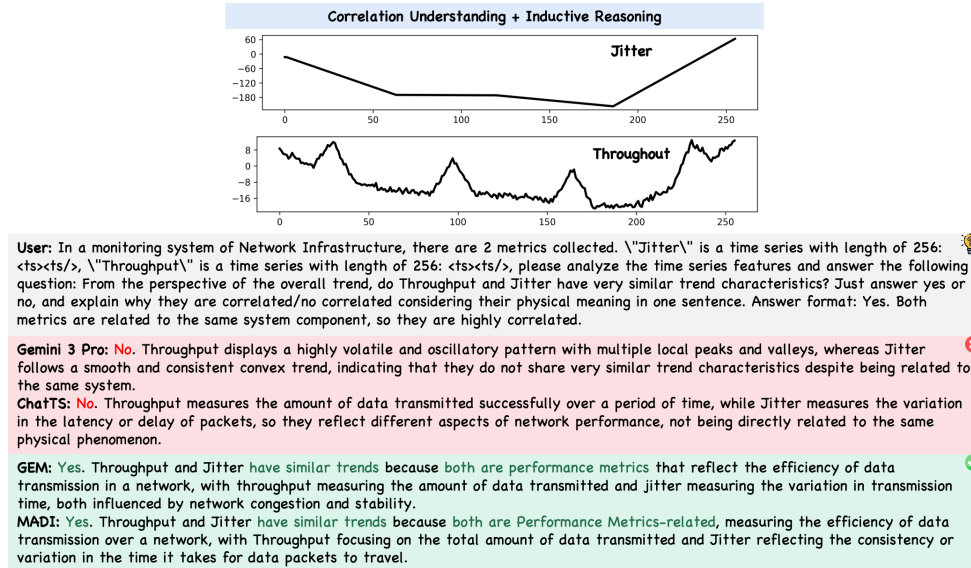


Figure 10. Case study of correlation understanding and inductive reasoning.

often rely on superficial signal characteristics (e.g., smoothness) or rigid definitions to incorrectly deny a relationship. MADI, conversely, looks past local signal disparities to identify the shared long-term trends driven by the underlying system physics. This confirms the model’s ability to perform semantic alignment between coupled time series variables.

Causal Reasoning. Figure 11 demonstrates a causal reasoning scenario using cost-per-click (CPC) data. The series features a precipitous drop around point 110, stabilizing at a lower level. MADI outperforms baselines by grounding its reasoning in domain logic, correctly attributing the shift to a “temporary drop in advertiser demand” and predicting a subsequent state of “stable market competition”. Other models, such as Gemini 3 Pro, hallucinate technical failures (“system misconfiguration”), revealing a lack of domain-aware causal inference.

Comparison Reasoning. Figure 12 involves a comparative analysis of influencer spike frequency across two video upload time series. A common pitfall for baselines is conflating signal amplitude with event frequency. Consequently, all baselines (Gemini 3 Pro, ChatTS, GEM) hallucinate an increased frequency in the “Updated” series due to its visual characteristics. MADI avoids this error, correctly observing that the spikes occur with the same frequency despite amplitude variations, effectively decoupling temporal rate from intensity.

Deductive Reasoning. Figure 13 tests the model’s ability to apply strict logical constraints to travel speed data, specifically regarding anomaly thresholds and noise patterns. While ChatTS and GEM fail to detect the anomaly, and Gemini 3 Pro fails to logically deduce the “typical” nature of the high-noise behavior in the follow-up question, MADI exhibits robust deductive capabilities. It explicitly verifies the amplitude condition ($54.14 > 50$) to detect the anomaly and correctly reasons that the observed fluctuations align with normal traffic variations given the problem’s specific constraints.

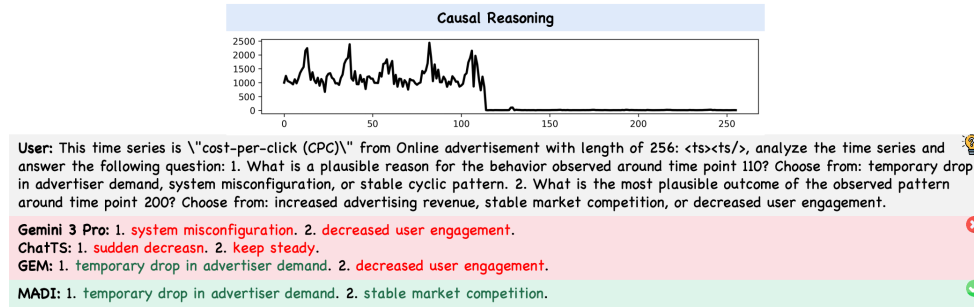


Figure 11. Case study of causal understanding.

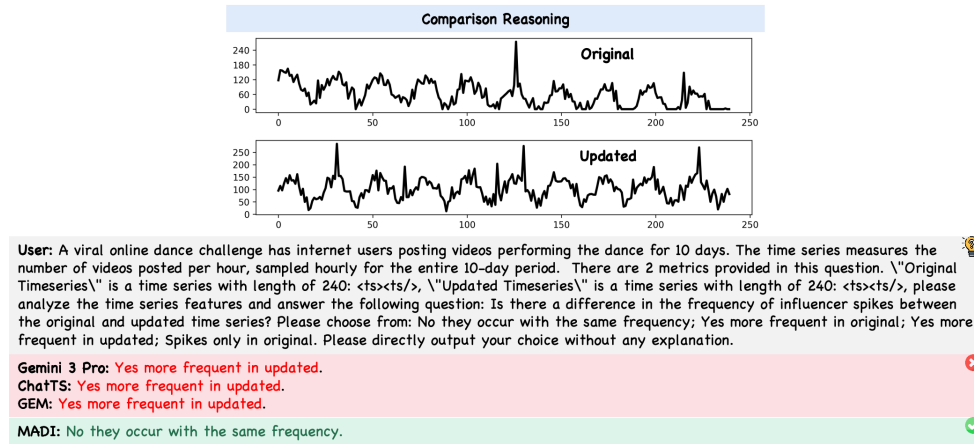


Figure 12. Case study of comparison understanding.



Figure 13. Case study of deductive understanding.